RSC Advances

ROYAL SOCIETY OF CHEMISTRY

www.rsc.org/advances

Mesoporous TUD-1 supported indium oxide nanoparticles for epoxidation of styrene using molecular O_2

Sumbul Rahman,[a] S. A. Farooqui,[b] Aditya Rai,[b] Rawesh Kumar,[a] Chiranjit Santra,[a] Vinod C Prabhakaran,[c] Gopala Ram Bhadu,[d] Debasis Sen,[e] S. Mazumder,[e] Sudip Maity,[f] Anil Sinha*[b] and Biswajit Chowdhury*[a]

Abstract: Activation of molecular O_2 by metal or metal oxide nanoparticle is being nurtured very recently. In this work, for the first time we report that indium oxide nanoparticles of <3 nm size dispersed on mesoporous silica (TUD-1) can activate molecular O_2 and produce styrene epoxide with a selectivity of 60 % and styrene conversion around 25 % at mild condition. It is found that neither indium oxide nor TUD-1 themselves respond to the styrene epoxidation reaction. The computational studies evidence that oxygen molecule is highly polarized when it is located near the interface of both surfaces. The kinetic study shows that reaction is of pseudo-first order and activation energy for styrene conversion is 12.138 kJ/mol. The catalysts are recyclable up to four regeneration steps keeping the styrene conversion and styrene epoxide selectivity almost unchanged.

1. Introduction

The investigations on metal oxide nanoparticles[1] are motivated by their wide range of properties that are useful for various applications including optics, electronics, magnetism and catalysts.[2] Indium oxide is an n-type semiconductor with a band gap (E_g = 3.70 eV) at room temperature. Research on indium oxide (In_2O_3) nanoparticles has attracted much attention in the recent years [3, 4] because of its applications in solar cell, field emission display, lithium ion battery, nanoscale bio-sensor, gas sensor, optoelectronics and photocatalysis.[5,6,7,8] Indium in its most stable oxidation state of (+III) is typically strong lewis acids because this species

possesses a vacant low energy orbital. As reported in the literature, indium (+III) is among the most commonly employed Lewis acids in the organic synthesis including asymmetric catalyst.[9]

Epoxides are very useful and versatile intermediates for the synthesis of many commodities and fine chemicals. The studies focusing on epoxidation of C=C bond have received much attention lately.[10,11,12] The traditional procedure for epoxidation of alkene using stochiometric amount of per-acids is not acceptable methodology from the environmental perspective.[13] The direct epoxidation using molecular O_2 is an atom economic pathway to get epoxides in mild conditions.[14] After successful production of ethylene epoxide over silver catalyst using molecular O_2 as an oxidant, many catalysts were developed in last two decades for epoxidation of higher homologous e.g. 1-3 butadiene, propylene etc.[15,16,17,18]

Styrene oxide is one of the most important fine chemical intermediates for producing perfume, drugs, sweeteners, epoxy resins etc. The current commercial production mostly employs the bromohydrin method, which gives rise to serious problems of equipment corrosion and environmental pollution.[19] The heterogeneous catalysts including Ti/SiO_2,[20] titanosilicate,[21] mixed metal oxide,[22] hydroxyapatites,[23,14] hydrotalcites[24] and cobalt doped mesoporous silica[25] were reported for this reaction. However, searching new catalyst system is being practiced, as commercial production of styrene epoxidation has not been developed so far using heterogeneous catalysts.

Ordered mesoporous materials with their intrinsically high surface area are excellently suited for catalytic materials towards various reactions. Compared to conventional carrier materials ordered mesoporous solids have the advantage of stabilizing dispersed metal or metal oxide nanoparticles.[26] TUD-1 is a mesoporous silica matrix with a large surface area and high thermal stability. Metal ions can be incorporated in the silica matrix which makes TUD-1 a potential catalyst candidate for several oxidation reaction including styrene epoxidation reactions.[27]

In this paper, for the first time, we report that indium oxide nanoparticles 2-3 nm size dispersed over TUD-1 material can activate molecular O_2 thereby producing styrene epoxide from styrene in mild condition. The two different indium doped TUD-1 (In/Si = 1/100 and 4/100) catalysts were prepared and characterized by N_2 adsorption-desorption isotherm, small angle X-ray scattering (SAXS), high resolution transmission electron microscopy (HRTEM), elemental mapping (STEM-EDS), fourier transform infrared spectroscopy (FTIR), X-ray photoelectron spectroscopy (XPS) and temperature programmed reduction (TPR), temperature programmed oxidation (TPO) techniques. The catalytic activity was optimized by varying flow of oxygen, temperature time of the reaction. The kinetic studies were carried out to find order, rate constant and activation energies of the reaction. Computational studies were carried to support the experimental results for activation of molecular O_2. An interesting correlation between catalytic activity and catalyst characterization results as well as theoretical studies is obtained as discussed later.

2. Materials and Methods

2.1. Preparation of In-TUD-1 Catalyst

In-TUD-1 catalyst was prepared by the non-hydrothermal sol-gel procedure as per literature.[27,28] In this procedure Tetraethylorthosilicate (TEOS, 98 %, Acros Organics) was mixed with aqueous solution of Indium nitrate (99.9 %, Aldrich) in deionized water under continuous stirring condition followed by the dropwise addition of Triethanolamine (TEA, 99 %, Acros Organics). Afterwards the whole mixture was stirred for 10 min and finally Tetraethylammonium hydroxide (TEAOH, 20 % aqueous solution, Merck, Germany) was added to keep the final gel composition of the mixture in the molar ratio of TEOS: $In(NO_3)_3$: TEA: H_2O: TEAOH= 1: x: 2: 11: 1. (x = 0.01, 0.04). The whole mixture was stirred for 24 h at room temperature and after stirring the prepared gel was dried at 110 °C for 24 h in a static air

oven. Finally the dried material was taken and calcined at the 700 °C for 10 h with a temperature increasing rate 1 °C/min in a muffle furnace (Thermcraft incorporated USA) .

2.2 Catalyst Characterization.

The nitrogen adsorption-desorption isotherms of the prepared catalysts was measured at liquid nitrogen temperature at -196 °C with a Quantachrome NOVA 3200, USA. Pre-treatment of the samples were done at 200 °C for 3 h under high vacuum. The surface area was calculated by Brunauer-Emmett-Teller (BET) equation and pore size distribution was calculated by the BJH method. Small angle X-ray scattering (SAXS) measurements were performed using a laboratory based SAXS instrument with Cu K_α X-ray radiation. The scattered intensities I(q) were recorded as a function of scattering vector q (= $4\pi \sin\theta/\lambda$, where 2θ is the scattering angle, and λ is the X-ray wavelength). The scattered intensity does not depend on the internal structure of the domains whether they are crystalline or amorphous.

To obtain the particle size distribution, SAXS data were analyzed in the light of polydispersed ensemble of spherical particles. For such a case, I(q) is expressed as

$$I(q) = C\left(\int_0^{\infty} P(q,R)D(R)R^6 dR\right)$$

where, P(q,R) represents the form factor of a spherical particle of radius R, i.e.,

$$P(q,R) = \frac{9(\sin(qR) - qRsin(qR))^2}{(qR)^6}$$

D(R) represents the particle size distribution, i.e., D(R)dR indicates the probability of having particle with radius R to R+dR. In the present case, a standard log normal distribution was assumed where C is a scale factor and does not depend on q.

The powder X-ray diffraction studies were performed on a Rigaku Ultima 4 X-ray diffractometer (JAPAN) with CuK_α radiation as X-ray source and data was analyzed by X'pert Highscore Plus software. The HRTEM image of the prepared catalysts was obtained on JEOL

JEM 2100 microscope (USA) operated at 200 KV acceleration voltage using lacey carbon coated Cu grid of 300 mesh size. The image J software was used to process TEM images in the figures. A random selection of 30 particles was used for size statics of the sample. The STEM was done using electron microscope model x-sight (Oxford instruments). The EDX measurements were done by Supra 55 (Zeiss, Germany) microscope equipped with Oxford instrument X-max detector and Gemini beam line attachment. The FT-IR measurements were carried out on a Perkin-Elmer spectrum two spectrophotometer (USA). The spectra were recorded in the wavelength range of 400-4000 cm^{-1} with 4 cm^{-1} energy resolution and samples were prepared using KBr pellet. The XPS was carried out using a custom built ambient pressure X-ray photoelectron spectrometer from PREVAC Inc (Poland). The spectra were collected at 50 eV pass energy using a monochromatic Al K_α X-ray source. All the binding energies of core electron were corrected using C(1s) core electron binding energy at 284.6 eV as reference. The quantification was done using CasaXPS software taking into consideration of atomic sensitivity factors of individual elements. The peaks were fitted using Shirley back ground correction. The TPR profiles of the catalysts were obtained from Chemisorb 2720 (Micrometrics, USA) instrument equipped with a TCD detector. The H_2-TPR profiles were obtained by reducing the catalyst samples with 10% H_2 in Ar at a flow rate of 20 mL/min and the temperature was increased from ambient to 800 °C at a rate of 10 °C/min. The TPO profiles of the samples were obtained using same equipment by oxidizing the catalyst samples with a gas mixture of 4.2 % O_2 in He with a flow rate of 20 mL/min and the temperature was increased from ambient to 800 ^oC at a rate of 10 ^oC/min. First, ~ 0.100 g of catalyst sample was dried with He flow in the preparation port of the instrument and dry mass was measured. Thereafter the experiment was carried out in the reaction port with the flow of the required gas mixture. In order to quantify the O_2 consumption, peak area of the respective samples was compared with a calibration file using Chemisoft (Micrometrics, USA) software.

2.3 Catalyst Activity Studies.

The In-TUD-1 catalysts were dried at room temperature in vacuum desicators, and used for the catalytic studies with no further activation. The catalytic reaction was studied in a batch reactor where 50 mL two necked round bottom flask was fitted with a water condenser. The reaction mixture was prepared by using 10 mL DMF (99.8 %, Merck, India), 6.5 mmol styrene (99 %, Acros Organics) and an internal standard dodecane (0.1 mL ,99 %, Across Organics). The reaction mixture was shaken vigorously for homogenization and 0.1 g catalyst was added to it. Then the prepared reaction mixture along with catalyst was kept in a heated silicon oil bath which was maintained at constant temperature (130 °C). Thereafter oxygen (99.99 % purity) was bubbled into the mixture at the flow rate of 10 mL/min (flow is maintained by Aalborg mass flow controller) under continuous stirring condition in a magnetic stirrer with 700 rpm rotational speed. The reaction mixture was analyzed by GC-1000 (Chemito-India) equipped with SE-30 column and FID detector. The detailed of GC condition has been provided in supporting information S1. The TOF per hour was calculated on the basis of moles of styrene converted /mol of indium present in the catalyst as determined by EDX and also based on oxygen uptake obtained from TPO experiment.

2.4 Kinetic Analysis.

The COMSOL muliphysics software (India), chemical species transport and reaction engineering module were used for simulation to validate the kinetics of experimental results.

2.5 Computational Details.

Molecular simulation studies were performed using Forcite module in Materials Studio 7.0 developed by Accelrys Software Inc.[29],[30] The structures were optimized by energy minimizing with Monte Carlo simulations using the Forcite module and the Condensed-Phase Optimized

Molecular Potentials for Atomistic Simulation Studies (COMPASS) force field was used in this work as implemented in Materials Studio and as was done earlier for similar systems.[29,31] The Forcite module is an advanced classical molecular mechanics tool that allows fast energy calculations and reliable geometry optimization of molecules and periodic systems.[32]

In the COMPASS force field, the total potential energy U is given by

$$U = U_b + U_\Theta + U_\Phi + U_\chi + U_{bb'} + U_{b\Theta} + U_{b\Phi} + U_{\Theta\Phi} + U_{b\Theta\Phi} + U_{coul} + U_{vdw}$$

The terms can be divided into two categories: valence terms, which include bond-stretching (U_b), bond-angle-bending (U_Θ), torsion (U_Φ), out-of-plane angle bending (U_χ), cross-coupling terms (bond-bond ($U_{bb'}$), bond- angle ($U_{b\Theta}$), bond-torsion ($U_{b\Phi}$), and bond-angle-torsion ($U_{b\Theta\Phi}$) interactions), and non-bonded interaction terms, which include the Coulombic function (U_{coul}) for electrostatic interactions and the Lennard-Jones 9-6 function (U_{vdw}) for van der Waals interactions.

To get accurate results, the crystal structures and atomic coordinates was optimized by minimizing the energy and atomic forces. Amorphous silicon oxide (SiO_2) was used as a base to impregnate indium oxide nanoparticles (cubic phase, 1 and 2 nm size). Forcite module was used for optimization of the structural geometry. Condensed-phase optimized molecular potentials for atomistic simulation studies (COMPASS) force field was used for the MD simulations. Interatomic potential force fields were automatically assigned for individual O and Si atoms as implemented in Material Studio while for In 'oxygen in metal oxide' force field was assigned. The COMPASS force field has been parameterized for molecules in isolation, in condensed phases, in metals and in metal oxides, to predict various properties such as dipole moment. To start the simulation, silica unit cell was imported from the library and the structure was optimized and relaxed to minimize its energy by using the Smart Minimizer method. The lower layers of silica were constrained. Indium oxide nanoparticles (Forcite, geometry optimized and fixed) were then stabilized on the silica surface along with oxygen molecules.

The silica surface was annealed from 300K to 973K . Oxygen molecules were brought in the close contact of different surfaces e.g. silica, indium oxide and at the interface of both silica- and indium oxide. Surface composition was $H_{500}O_{1728}Si_{864}$ for 2 nm thickness silica slab. For 1 nm In_2O_3 nanoparticle surface composition was $In_{14}O_{24}$.

After performing forcite geometry optimization, the charge induced on individual atoms was calculated using charge equilibration method (QEq) in Forcite. Conditions for simulation were: Force: 0.5 kcal/mol/Å; Temperature: 383K Maximum number of iterations: 500; Energy parameters -Forcefield: COMPASS (Version 2.8); Charges: Forcefield assigned; Electrostatic terms & van der Waals terms - Summation method: Atom based; Truncation method: Cubic spline; Cutoff distance: 12.5 Å; Spline width: 1 Å; Buffer width: 0.5 Å.

For comparison, the simulation was also carried using Universal Force Field (UFF), another more simplistic approach, available in Material Studio. In the UFF force field, the total potential energy U is given by

$$U = U_b + U_\Theta + U_\Phi + U_{vdw}$$

where U_b represents the bond-stretching interactions, U_Θ represents the angle-bending interactions, U_Φ represents the torsional interactions, and U_{vdw} represents the non-bonded interactions.

Amorphous silica surface was taken from standard Material Studio library, SiO_2 surface was 16 Å thick layer with composition $H_{140}Si_{436}O_{868}$ and a surface composition of $H_{69}Si_{51}O_{104}$. Silica surface and Indium oxide nanoparticles (1 nm and 2 nm) was annealed from 300-973 K using UFF force field. Cutoff voltage and inter atomic potentials were force field assigned as implemented in Material Studio software. For nonbonding interaction, the electrostatic interaction was based on Ewald method and van-der-waals interaction was atom based during

the calculation. Indium oxide nanoparticles (1 nm and 2 nm) were brought near SiO_2 (amorphous) surface and was further optimized using UFF method. To calculate charge on individual atoms of oxygen molecule, oxygen was brought in the vicinity of finalized structure (indium doped on silica surface) at different locations. The charge was calculated using charge equilibrartion (Qeq) method. Before performing qEQ method the structure was neutralized.

3. RESULT AND DISCUSSION

3.1 N_2 Adsorption-Desorption Isotherm.

The textural characteristics of TUD-1 and In-TUD-1 catalysts with different indium loading were listed in Table 1. The materials exhibited a high BET surface area, a large pore volume and a porosity exclusively of mesopores as illustrated by the nitrogen sorption isotherms (Fig. 1**)**. From the Table 1, it was found that with the increase in indium loading there was a decrease in surface area and pore volume which might be due to the blocking of mesopores by indium oxide nanoparticles as reported in the literature.[33]

3.2 Small Angle X-ray Scattering (SAXS).

To find a better insight about the particle size distribution of the In-TUD-1 catalysts the SAXS analysis was carried out.[34,35] The SAXS profiles of the In-TUD-1 catalysts is shown in Fig. 2. The increasing trend of intensity at low q regime for samples In-TUD-1(In/Si = 1/100) and In-TUD-1 (In/Si = 4/100) catalysts, was observed. It is to be mentioned that such increase in scattering at low q regime was originated from the density fluctuations at larger length scale. This might be either due to the agglomeration of the primary particles or due to the presence of the pores. Thus, another size distribution and a power law contribution were also considered while modeling. For sample with (In/Si = 1/00), only a power law type increase was observed

and thus estimation of larger size distribution could not be possible. The plot of size distribution vs. radius of the primary particles is shown in Fig. 2. The specific surface area of TUD-1 increased with indium doping however at higher indium loading specific surface area decreased (Table 2) which is in agreement of N_2-physisorption studies.

3.3 X-ray Diffraction (XRD).

XRD pattern of In-TUD-1 (In/Si = 1/100) showed the absence of diffraction peaks for crystalline indium oxide (Supporting Information Fig. S2); however in higher loading i.e. In-TUD-1 (In/Si = 4/100) typical diffraction peaks at (222), (400), (440), and (622) appeared due to the presence of cubic In_2O_3 species (JCPDS Card No. 00-006-0416).

3.4 High Resolution Transmission Electron Microscope (HRTEM) and Elemental Mapping by STEM-EDS Analysis.

HRTEM analysis was employed to study the morphology of nanoparticles as well as to provide evidence on their distribution throughout the mesoporous silica matrix. The three dimensional spongelike morphology[17] is evident from HRTEM image (Supporting Information Fig. S3) and particle size distribution (Fig. 3) of In-TUD-1 catalysts (In/Si = 1/100, and 4/100). The nanoparticles of 2-3 nm size well dispersed in the spongelike matrix was observed for In-TUD-1 catalysts (In/Si = 1/100, and 4/100).

As observed in Fig. 3, the average size of the nanoparticles is bigger for In-TUD-1 (In/Si = 4/100); compared to lower indium loading (In/Si = 1/100). The nuclei formation and subsequent growth in the sol-gel synthesis were largely depended on the concentration of precursor salt during synthesis.[36] The formation of bigger particles strengthened the observation derived from N_2-physisorption, SAXS studies in the earlier section.

The presence of indium in the TUD-1 matrix was confirmed by STEM analysis as shown in Fig. 4. The uniform distribution of indium in In-TUD-1 (In/Si = 1/100) was also obtained.

The Si and O atomic mapping confirmed the sustaining of the spongelike matrix in In-TUD-1 (In/Si = 1/100) catalyst however at higher loading (In/Si = 4/100) of indium the spots were more localized.

3.5 Fourier Transform Infrared (FT-IR) Spectra.

The FT-IR spectra of indium doped and undoped TUD-1 catalysts are shown in supporting information (Fig. S4). A strong adsorption band was found at 960 cm^{-1} which was due to the stretching frequency of terminal silanol (Si-OH) group. The bands at 1090 and 804 cm^{-1} indicated the framework vibrations, which were assigned to the asymmetric and symmetric stretching vibrations of Si–O–Si bridges, respectively.[37]

In case of In-TUD-1 (In/Si= 4/100) the band at 804 cm^{-1} has the lowest intensity because of high percentage of indium metal incorporated into the TUD-1 matrix with successive formation of Si-O-M (M = In) moiety.[25] In the hydroxyl region, the weak band at 1637 cm^{-1} and the broad band at 3470 cm^{-1} could be attributed to the combination of stretching vibration of silanol groups or silanol ‘‘nests” with cross hydrogen-bonding interactions and the H–O–H stretching mode of physisorbed water present in the prepared catalysts.

3.6 X-ray Photoelectron Spectroscopy (XPS).

The XPS analysis was carried out to determine the core electron binding energy (BE) values of the corresponding elements present in In-TUD-1 catalysts. The O (1s) core level XPS spectra of TUD-1 and In-TUD-1 catalysts with two different indium loadings are shown in Fig. 5. As reported in the literature, for the mixed oxides, the O (1s) peak was appeared in the range of 530.6-534.5 eV for the M-O-M' bond where M and M' were two metals of different electronagativity.[38,39,40] In the present case, for two In-TUD-1catalysts, the O (1s) peak appeared in the range between 532.9-533.4 eV which was due to the covalent oxygen present

in Si–O–Si bond. As only one O (1s) peak was observed in the present case, so it could be inferred that isolated indium species was highly dispersed on the silica matrix.

The Si (2p) core level XPS spectra for two different samples i.e. TUD-1 and In-TUD-1 catalysts are shown in Fig. 6. The peak at 104.4 eV indicated that silica was present in its +4 oxidation state[18] in the In-TUD-1 (In/Si = 4/100) catalyst which is similar for other metal substituted TUD-1 catalyst.

The In (3d) core level XPS spectra of the prepared catalysts are shown in Fig 7. The peak maximum for $3d_{5/2}$ was centered on 445 eV implying the existence of indium in its +3 oxidation state in the In-TUD-1 catalyst. No peak around 444 eV due to metallic indium was observed by peak fitting of the XPS spectra.6 For In-TUD-1 catalyst (In/Si = 4/100) the peak of oxidized indium species was shifted to lower binding energy value. From the observed shift of Si (2p) and In (3d) binding energy values it can be said that nature of electronic interaction was different for In-TUD-1 (In/Si = 1/100) catalysts compared to higher indium loading. The quantitative XPS result (Table 3) showed that the surface concentration of Indium was lower for In-TUD-1 (In/Si = 4/100) compared to In-TUD-1 (1/100) catalyst. The concentration of surface oxygen species was almost similar in both the cases. As the activity was changed due to the change in surface indium species so that it might be said that In/Si perimeter interface was the active center to generate electrophilic oxygen species from molecular oxygen. For the In-TUD (In/Si = 1/100) catalyst the smaller nanoparticles had more contact area in the perimeter interface resulting higher catalytic activity as described later.[41]

3.7 Temperature Programmed Reduction (TPR) Studies.

Two main reduction peaks in the temperature range between 450-650 °C are shown in the TPR profile of different indium loaded TUD-1 (Fig. 8). The appearance of the reduction peak in the temperature range between 450-525 °C might be due to the reduction of the highly dispersed

indium species formed during the preparation of In-TUD-1 catalysts because of the strong interaction between surface indium species and the protonic acid sites of TUD-1 material.[42] The H_2 uptake peak around 550-650 °C could be assigned to the reduction of large grained In_2O_3 crystallite phase.[43] As evident from TPR profile, the In_2O_3 species were highly dispersed in case of In-TUD-1 (In/Si = 1/100) catalyst but in case of In-TUD-1 (In/Si = 4/100) catalyst, the indium oxide species were agglomerated on the surface of TUD-1 material.

3.8 Temperature Programmed Oxidation (TPO) Studies.

The TPO profile of In-TUD-1 catalysts is shown in Fig. 9. At higher loading, O_2 consumption per gram catalyst was dropped steeply and also oxygen chemisorptions peak was shifted to higher temperature (Table 4). The TPO observation indicated that the active sites were accessible at lower loading whereas at higher loading the amount of oxygen uptake was less.

4. Catalytic activity studies

The catalytic activity of In-TUD-1 catalysts with two different amounts of indium loaded TUD-1 catalyst (In/Si = 1/100; 4/100) towards the epoxidation reaction of styrene by using molecular O_2 is shown in Table 5. The maximum conversion of styrene and also the selectivity of styrene oxide was observed in In-TUD-1 (In/Si = 1/100) catalyst compared to other indium loaded TUD-1 (In/Si = 4/100) catalyst. The product was obtained only in case of using DMF as solvent (supporting information Table S5). The increased styrene conversion for In-TUD-1 (In/Si = 1/100) catalyst might be due to the homogeneous distribution of indium oxide nanoparticles over the TUD-1 matrix which is supported by high resolution TEM images (supporting information, Fig. S3) for In-TUD-1 (In/Si = 1/100) catalyst. The lower TOF value at higher indium loading might be due to the less accessibility of indium active sites and agglomeration of the particles as supported by HRTEM results. An interesting observation was found when TOF was calculated based on moles of indium present as well as amount of

oxygen uptake. The TOF value was calculated considering indium content was higher in the case of In-TUD-1 (In/Si = 1/100) compare to In-TUD-1 (In/Si = 4/100). However the TOF was calculated based on oxygen uptake during TPO experiment was lower for In-TUD-1 (In/Si = 1/100) with respect to In-TUD-1 (In/Si = 4/100). So it is obvious that oxidizing sites were not solely the active sites. The acidity of In-TUD-1 (In/Si = 4/100) was found higher than In-TUD-1 (In/Si = 1/100) catalyst as found from NH_3-TPD result (Supporting Information Fig S6). This implies that the acidic sites due to In (III) took part in the reaction enhancing the hydrolysis of styrene epoxide to benzaldehyde as shown in the Table 5.

4.1 Effect of Reaction Temperature.

The influence of reaction temperature on the oxidation of styrene with molecular O_2 over In-TUD-1 (In/Si = 1/100) catalyst is shown in Table 6. The conversion of styrene was increased with the increase in reaction temperature at the beginning. For example, styrene conversion was 11.26 % at 70 °C and it quickly rose to 24.76 % at 130 °C temperature. With further increase of temperature styrene conversion and selectivity were lowered as shown in Table 6. Expectedly, TOF value was increased with the temperature because of more styrene conversion. As reported in the literature[25] at higher temperature the rate of styrene epoxidation reaction was determined by the diffusion of reactants to the active sites. The decrease of selectivity of styrene oxide at higher temperature might be due to the epoxide ring opening reaction. From this experimental result it seems that an appropriate reaction temperature is essential to obtain maximum styrene oxide selectivity.

4.2 Effect of O_2 Flow Rate.

A significant effect on the catalytic performance by variation of molecular oxygen is shown in Table 7. It is found that after 10 mL/min O_2 flow rate, styrene conversion had little change but styrene oxide selectivity was dropped continuously. This indicated that at 10 mL/min O_2 flow,

an optimum styrene conversion was reached but selectivity to styrene oxide was decreased continuously at higher O_2 flow. However, the TOF value was remained constant with O_2 flow.

4.3 Effect of Regeneration.

The catalyst recyclability is one of the important parameter for catalyst commercialization. Deactivated In-TUD-1 (In/Si = 1/100) catalyst was regenerated by washing with acetone and dried overnight at 80 ^oC temperature. The catalytic activity was steady upto four regeneration cycle over In-TUD-1 (In/Si = 1/100) catalyst as is presented in Fig. 10.

4.4 Kinetic Studies.

For the kinetic studies styrene was taken in a batch reactor at temperature 130 ^oC and O_2 was passed continuously at flow rate of 10 ml/min. For different styrene reaction orders, the rate constant was calculated and it was found that for order n = 1, the data obtained experimentally fits well with the calculated one. The corresponding rate constant (k) for the reaction was 0.027 h^{-1} (supporting information Table S7 and Fig. S8). R^2 values (Table S7) and best fit (in Figure S8) were used as the criteria for the selection of reaction order. The plot of simulated and experimental conversions showed that the best fit was obtained considering psuedo-first order kinetics for styrene conversion (Fig. 11). The apparent activation energy for the reaction was 12.138 kJ/mol (supporting information Table S9 and Fig. S10).

5. Theoretical Calculation

In order to confirm the necessity of indium nanoparticles on silica surface for oxygen activation, the computational studies were undertaken. The optimized structure representing In_2O_3 nanoparticles on SiO_2 surface in the presence of oxygen molecules is given in Fig. 12. After stabilizing In_2O_3 nanoparticle on SiO_2 surface O_2 molecule was used as adsorbate for this new structure.

Potential functions can estimate charge distribution correctly. Charge distribution is a crucial indicator of molecular reactivity. Charge equilibration method (QEq) was used to calculate the charges of atoms. The charges of atoms in oxygen molecule were assigned to show that the charges on oxygen atoms of adsorbed oxygen molecules were influenced (charges are polarized/delocalized) by the presence of indium oxide nanoparticles on silica surface indicating oxygen activation. It was observed that the charge on oxygen atoms in molecule was varied depending on its location. Minimum charge polarization on O_2 (δq: $\leq$ 0.05) was induced when the oxygen molecule was in the close proximity of silica surface only, and maximum charge polarization on O_2 (δq: 0.2) was induced near indium oxide. The simulation results using COMPASS force field method were further corroborated with a more simplistic approach using UFF force field method (Supporting Fig. S11). It was clearly observed that very little polarization of oxygen molecules occurred in the silica surface (Δq: 0.03-0.09), while the oxygen molecules around the indium oxide nanoparticle on silica surface were prominently polarized (Δq: 0.2-2.0). It may be concluded that oxygen molecule was highly polarized when it was near the indium oxide stabilized on silica surface. Active oxygen species formation occur through reductive activation of di-oxygen (generally) at catalyst surfaces; for semiconducting oxides the metal sites of oxygen activation become progressively more oxidized., consequently, the bonding interaction between oxygen and metal site becomes progressively stronger[44] Molecular oxygen polarization may be an indicator of its activation. Thus, our calculations indicate that surface decoration of silica with indium oxide nanoparticles resulted in oxygen activation.

6. Conclusion

In conclusion we demonstrated the direct styrene epoxidation reaction using molecular O_2 as an oxidant over In-TUD-1 catalyst. For the first time it is found that indium oxide nanoparticles can activate molecular O_2 only when dispersed over silica matrix. The electronic interaction differed for the higher loading of indium as evident from XPS studies. The catalytic activity studies showed that the lower loading of indium had better activity towards styrene epoxidation reaction. The computational study showed the molecular O_2 was polarized when indium oxide nanoparticle was dispersed over silica surface. Little polarization of O_2 molecule was obtained on the bare silica surface. The research on the activation of molecular O_2 by indium oxide might contribute to research towards several other oxidation reactions such as photocatalytic oxidation of water for production of hydrogen.

Acknowledgements

BC would like to acknowledge DST Govt. of India for research grant (scheme SB/S1/PC-10/2012) and DST Govt. of India for research grant (INT/NL/FM/P-002/2013). CS and SR acknowledge UGC for research fellowship. RK wants to acknowledge ISM for providing research fellowship.

Notes and references

[a] Department of Applied Chemistry, Indian School of Mines (ISM), Dhanbad

[b] CSIR-Indian Institute of Petroleum (IIP), Dehradun, India

[c] Catalysis Division and Center of Excellence on Surface Science, National Chemical Laboratory (NCL), Pune, India

[d] Analytical Division, Central Salt & Marine Chemicals Research Institute (CSMCRI) Bhavnagar, India

[e] Solid State Physics Division, Bhabha Atomic Research Center (BARC), Mumbai, India

[f] Central Institute of Mining and Fuel Research (CIMFR), Dhanbad, India

Corresponding authors:

[*a] Email: biswajit_chem2003@yahoo.com, Tel.: +91-326-2235663; fax: +91-326-2296563.

[*b] Email: asinha@iip.res.in, Tel.: +91-135-2525842.

1. B. M. Reddy and B. Chowdhury, *Langmuir*, 2001, **17**, 1132–1137.

2. N. H. Chou, X. Ke, P. Schiffer and R. E. Schaak, *J. Am. Chem. Soc*., 2008, **130**, 8140–8141.

3. C. Shifu, Yu. Xiaoling, Z. Huaye and L. Wei. *J. Hazard. Mater.*, 2010, **180**, 735– 740.

4. (a) D. B. Buchholz, Q. Ma, D. Alducin, A. Ponce, M. J. Yacamán, R. Khanal, J. E. Medvedeva and R. P. H. Chang, *Chem. Mater.*, 2014, **26**, 5401–5411. (b) V. D. Ashok and S. K. De, *J. Phys. Chem. C*, 2011, **115**, 9382–9392.

5. J. Chandradass, D. S. Bae and K. H. Kim, *Adv. Powder Technol.,* 2011, **22**, 370–374.

6. Z. M. Detweiler, J. L. White, S. L. Bernasek and A. B. Bocarsly, *Langmuir,* 2014, **30**, 7593–7600.

7. J. Du, M. Yang, S. N. Cha, D. Rhen, M. Kang and D. J. Kang, *Cryst. Growth Des*., 2008, **8**, 2312–2317.

8. M. Kumar, V. N. Singh, B. R. Mehta and J. P. Singh, *J. Phys. Chem., C,* 2012, **116**, 5450–5455.

9. U. Schneider and S. Kobayashi, *Acc. Chem. Res.,* 2012, **45**, 1331–1334.

10. S. Jana, B. Dutta, R. Bera and S. Koner, *Langmuir*, 2007, **23**, 2492–2496.

11. B. Singh and A. K. Sinha, *J. Mater. Chem. A,* 2014, **2**, 1930–1939.

12. W. Li, Y. Gao, W. Chen, P. Tang, W. Li, Z. Shi, D. Su, J. Wang and D. Ma, *ACS Catal*., 2014, **4**, 1261–1266.

13. J. M. Judge, 1971, **2**, 963.

14. Z. Opre, T. Mallat and A. Baiker, *J. Catal.,* 2007, 245, 482–486.

15. B. Chowdhury, J. J. Bravo Suarez, M. Date, S. Tsubota and M. Haruta, *Angew. Chem. Int. Ed.*, 2006, **45**, 412–415.

16. J. R. Monnier, *Appl. Catal. A: Gen.,* 2001, **221**, 73– 91 and references therein.

17. A. K. Sinha, S. Seelan, S. Tsubota and M. Haruta, *Angew. Chem. Int. Ed*., 2004, **43**, 1546–1548.

18. A. K. Sinha, S. Seelan, M. Okumura, T. Akita, S. Tsubota and M. Haruta *J. Phys. Chem. B,* 2005, **109**, 3956–3965.

19. X. Yang, S. Gao and Z. Xi, *Org. Process Res. Dev.,* 2005, **9**, 294–296.

20. Q. Yang, S. Wang, J. Lu, G. Xing, Z. Feng, Q. Xin and C. Li, *Appl. Catal. A: Gen.,* 2000, **194**, 507–514.

21. S. B. Kumar, S. P. Mirajkar, C. G. Paris, P. Kumar and R. Kumar. *J. Catal.,* 1995, **156**, 163–166.

22. N. Ma, Y. Yue, W. Hua and Zi. Gao. *Appl. Catal. A: Gen.,* 2003, **251**, 39–47.

23. K. Yamaguchi, K. Ebitani and K. Kaneda, *J. Org. Chem.,* 1999, **64**, 2966–2968.

24. I. Kirm, F. Medina, X. Rodriguez, Y. Cesteros, P. Salagre and J. Sueiras, *Appl. Catal. A: Gen.,* 2004, **272**, 175–185.

25. S. Rahman, C. Santra, R. Kumar, J. Bahadur, A. Sultana, R. Schweins, D. Sen, S. Maity, S. Mazumdar and B. Chowdhury, *Appl. Catal A: Gen.,* 2014, **482**, 61–68.

26. Y. Li, Guan, R. A. van Santen, P. J. Kooyman, I. Dugulan, C. Li and E. J. M. Hensen, *J. Phys. Chem. C,* 2009, **113**, 21831–21839.

27. S. Mandal, S. Rahman, R. Kumar, K. K. Bando and B. Chowdhury. *Catal. Commun.,* 2014, **46**, 123–127.

28. S. Mandal, A. M. Sinha, B. Rakesh, R. Kumar, A. Panda and B. Chowdhury, *Catal. Commun.,* 2011, **12**, 734–738.

29. http://accelrys.com/products/materials-studio/index.html

30. S. Chang, T. Yoshioka, M. Kanezashi, T. Tsuru, K. Tung, *Chem. Commun.,* 2010, **46**, 9140-9142.

31. Tudor C. Ionescu, F Qi, C McCabe, A Striolo, J. Kieffer, and Peter T. Cummings; *J. Phys. Chem. B* 2006, 110, 2502-2510

32. B. P. C. Hereijgers, T. M. Eggenhuisen, K. P. de Jong, H. Talsma, A. M. J. van der Eerden, A. M. Beale, Bert M. Weckhuysen. *J. Phys. Chem. C,* 2011, **115**, 15545–15554.

33. A. Ramanathan, T. Archipov, R. Maheswari, U. Hanefeld, E. Roduner and R. Roger Glaser. . *J. Phys. Chem. C,* 2008, **112**, 7468–7476.

34. D. Sen, S. Mazumder, J. S. Melo, A. Khan, S. Bhattyacharya and S. F. D'Souza, *Langmuir,* 2009, **25**, 6690–6695.

35. D. Sen, J. Bahadur, S. Mazumder and P. S. Bhattacharya, *Soft Matter.,* 2012, **8**, 10036–10044.

36. G. J. A. A. Soler-Illia, C. Sanchez, B. Lebeau and J. Patarin, *Chem. Rev.,* 2002, **102**, 4093–4138.

37. A. Bordoloi and S. B. Halligudi, *J. Catal.,* 2008, **257**, 283–290.

38. S. Mandal, K. K. Bando, C. Santra, S. Maity, O. O. James, D. Mehta and B. Chowdhury, *Appl. Catal. A Gen.,* 2013, **452**, 94–104.

39. B. M. Reddy, B. Chowdhury, I. Ganesh, E. P. Reddy, T. C. Rojas and A. Fernandez, *J. Phys. Chem.,* 1998, **102**, 10176–10182.

40. C. Santra, S. Rahman, S. Bojja, S. Maity, D. Sen, O. O. James, A. K. Mohanty, S. Mazumder and B. Chowdhury, *Catal. Sci. Technol.,* 2013, **3**, 360–370.

41. B. Chowdhury, J. J. Bravo-Suárez, N. Mimura, Jiqing, K. K. Bando, S. Tsubota, and M. Haruta *J. Phys. Chem. B*, 2006, **110** (46), 22995–22999.

42. X. Zhou, X. Xu, T. Zhang and L. Lin, *J. Mol. Catal. A: Chem*., 1997, **122**, 125–129.

43. P. W. Park, C. S. Ragle, C. L. Boyer, M. Lou Balmer, M. Engelhard and D. McCready, *J. Catal*., 2002, **210**, 97–105.

44. R. Schlögl, Concepts in Selective Oxidation of Small Alkane Molecules, in Modern Heterogeneous Oxidation Catalysis: Design, Reactions and Characterization (ed N. Mizuno) Wiley-VCH Verlag GmbH & Co. KGaA, Weinheim, Germany.
doi: 10.1002/9783527627547.ch1(2009)

Figure captions

Fig. 1 Surface area and porosity measurement of (a) TUD-1 (b) In-TUD-1 (In/Si = 1/100) (c) In-TUD-1 (In/Si = 4/100) catalysts

Fig. 2 Fitting of the model to the experimental SAXS data. Solid line represents the fit in each case.

Fig. 3 Particle size distribution of In-TUD-1 (a) In/Si = 1/100 and (b) In/Si = 4/100 catalysts as obtained for HRTEM analysis.

Fig. 4 Elemental mapping by STEM analysis of (a) In-TUD-1 (In/Si = 1/100), (b) In- TUD-1 (In/Si = 4/100) catalysts.

Fig. 5 The O (1s) core level XPS spectra of (a) TUD-1 (b) In-TUD-1 (In/Si = 1/100) (c) In-TUD-1 (In/Si = 4/100) catalyst.

Fig. 6 Si (2p) core level XPS spectra of (a) TUD-1 (b) In-TUD-1 (In/Si = 1/100) (c) In-TUD-1 (In/Si = 4/100) catalyst.

Fig. 7 In (3d) core level XPS spectra of (a) In-TUD-1 (In/Si = 1/100) (b) In-TUD-1 (In/Si = 4/100) catalysts

Fig. 8 The H_2-TPR profiles of (a) TUD-1 (b) In-TUD-1 (In/Si = 1/100) (c) In-TUD-1 (In/Si = 4/100) catalysts.

Fig. 9 The TPO profile of (a) In-TUD-1 (In/Si = 1/100), (b) In-TUD-1 (In/Si = 4/100) catalysts.

Fig. 10 Activity results of regenerated In-TUD-1 (In/Si = 1/100) catalyst for styrene epoxidation reaction.

Fig. 11 Plot of Simulated and Experimental conversion (%) vs. Time (h) for styrene epoxidation reaction in a batch reactor.

Fig. 12 The optimized structure for O_2 as adsorbate on SiO_2 surface with In_2O_3 nanoparticle along with partial charges on the atoms of adsorbed oxygen.

Tables

Table 1. Surface area and Pore diameter of different In-TUD-1 catalyst

Catalyst	Surface Area (m^2/g)	Total pore volume (cc/g)	Pore Diameter (nm)
TUD-1	452.3	0.859	7.60
In-TUD-1 (In/Si= 1/ 100)	688.7	1.094	8.30
In-TUD-1 (In/Si= 4/ 100)	663.4	0.834	7.22

Table 2. Quantitative analysis of SAXS results for In-TUD-1 catalyst.

Catalyst	Average diameter (nm)	Σ (m^{-1})	Calculated theoretical density of the samples (with d_{silica} = 2 g/cc and d_{In} = 7.3 g/cc)	Σ (m^2/g) [assuming the calculated theoretical density]
TUD-1	2.8	2.25×10^9	2.00	1090
In-TUD-1 (In/Si= 1/ 100)	2.2	3.13×10^9	2.05	1525
In-TUD-1 (In/Si= 4/ 100)	1.9	3.30×10^9	2.20	1500

Table 3. Quantitative XPS data for the In-TUD-1 catalyst

Catalyst	In (3d)	Si (2p)	O (1s)
	At. %	At. %	At. %
In-TUD-1 (In/Si = 1/100)	0.03	38.8	56.85
In-TUD-1 (In/Si = 4/100)	0.01	41.0	56.34

Table 4. Temperature Programmed Oxidation (TPO) results of In-TUD-1 catalyst.

Catalyst	Peak Temperature (^oC)	O_2 uptake (μmole/g)
In-TUD-1 (In/Si= 1/ 100)	89.8	140.1
In-TUD-1 (In/Si= 4/ 100)	120.5	53.21

Table 5. Catalytic data for In-TUD-1 catalyst for Styrene epoxidation reaction at different indium loading.

Catalyst	Conversion (%)	Selectivity (%)		Indium % as per EDX		O_2 uptake (μmole/g)	TOF* $(h^{-1})^a$	TOF* $(h^{-1})^b$
		Styrene Oxide	Benzaldehyde	Wt%	At%			
In-TUD-1 (In/Si= 1/ 100)	16.6	45.5	54.5	3.61	0.63	140.1	4.5	1.5
In-TUD-1 (In/Si= 4/ 100)	14.4	32.3	67.7	7.80	1.42	53.21	1.7	2.2

Reaction conditions: DMF, 10 mL; Styrene, 6.5 mmol; Dodecane, 0.1 mL; catalyst, 0.1 g; O_2 flow rate, 10 mL min^{-1}; Reaction time, 8h; *TOF = moles of styrene converted /moles of indium present in the catalyst per gram/hour [where a: as per indium content and b: as per oxygen uptake]

Table 6. Catalytic data for In-TUD-1 (In/Si = 1/100) catalyst for Styrene epoxidation reaction at different temperature.

Catalyst	Temperature (^oC)	Conversion (%)	Selectivity (%)		TOF* $(h^{-1})^a$	TOF* $(h^{-1})^b$
			Styrene Oxide	Benzaldehyde		
In-TUD-1	70	11.2	32.1	67.8	3.0	0.65
In-TUD-1	90	14.6	42.1	57.8	4.0	0.85
In-TUD-1	110	16.5	45.4	54.5	4.3	1.00
In-TUD-1	130	24.7	57.0	42.9	6.4	1.43
In-TUD-1	150	23.0	54.3	45.7	6.0	1.33

Reaction conditions: DMF, 10 mL; Styrene, 6.5 mmol; Dodecane, 0.1 mL; catalyst, 0.1 g; O_2 flow rate, 10 mL min^{-1}; Reaction time, 8h; *TOF = moles of styrene converted /moles of indium present in per hour [where a: as per indium content and b: as per oxygen uptake]

Table 7. Catalytic data for In-TUD-1 (In/Si = 1/100) catalyst for Styrene epoxidation reaction at different O_2 flow.

Catalyst	O_2 flow mL min^{-1}	Conversion (%)	Selectivity (%)		TOF* $(h^{-1})^a$	TOF* $(h^{-1})^b$
			Styrene Oxide	Benzaldehyde		
In-TUD-1	5	22.0	56.2	43.7	6.0	1.30
In-TUD-1	10	24.7	57.0	42.9	6.4	1.43
In-TUD-1	20	24.6	54.4	45.5	6.4	1.43
In-TUD-1	25	23.7	53.9	46.1	6.2	1.40

Reaction conditions: DMF, 10 mL; Styrene, 6.5 mmol; Dodecane, 0.1 mL; catalyst, 0.1 g; Reaction temperature, 130 ^oC; Reaction time, 8h; *TOF = moles of styrene converted /moles of indium present in the catalyst per hour [where a: as per indium content and b: as per oxygen uptake]

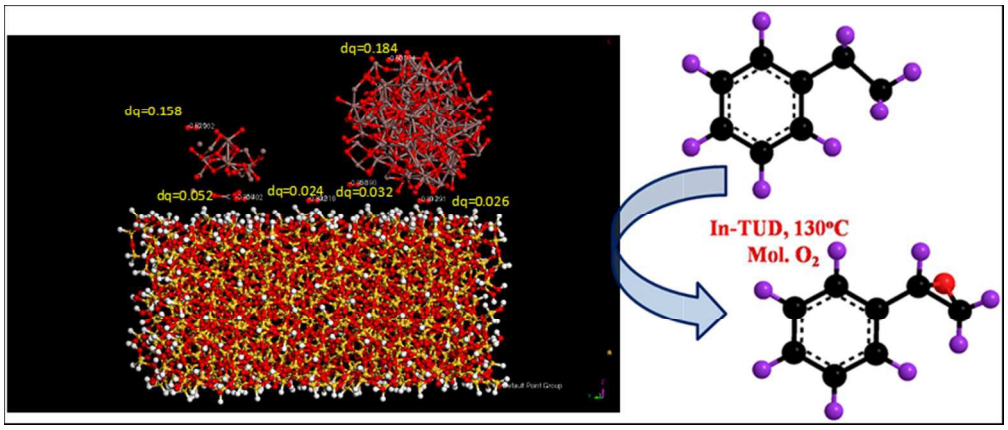

227x95mm (96 x 96 DPI)

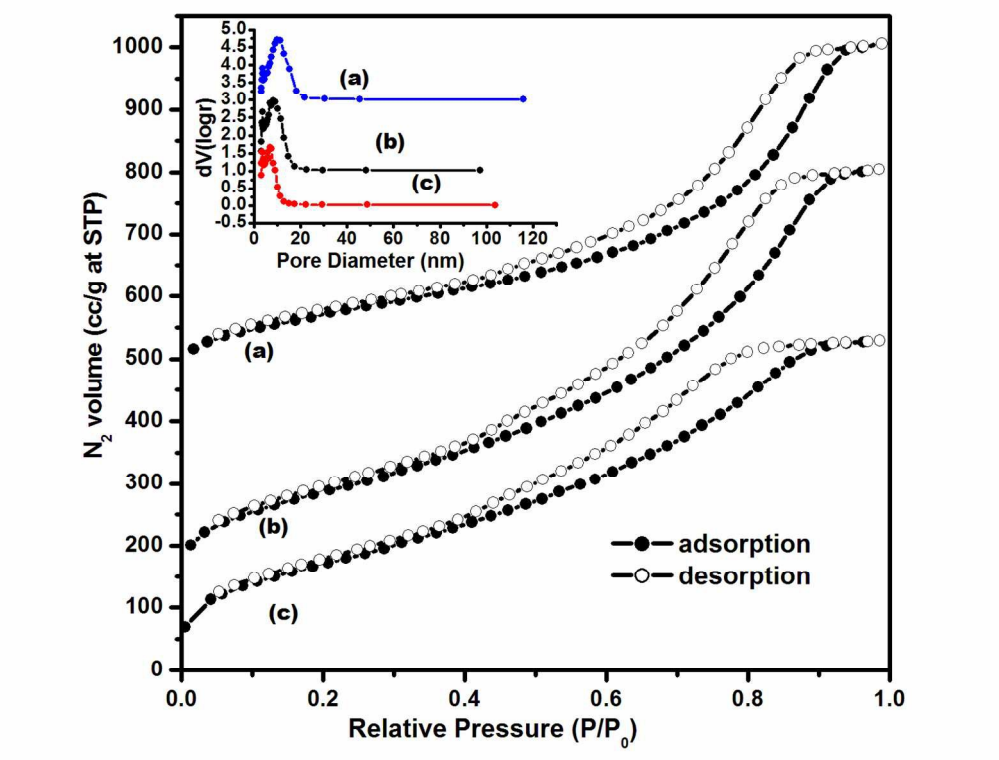

Fig. 1 Surface area and porosity measurement of (a) TUD-1 (b) In-TUD-1 (In/Si = 1/100) (c) In-TUD-1 (In/Si = 4/100) catalysts
270x206mm (150 x 150 DPI)

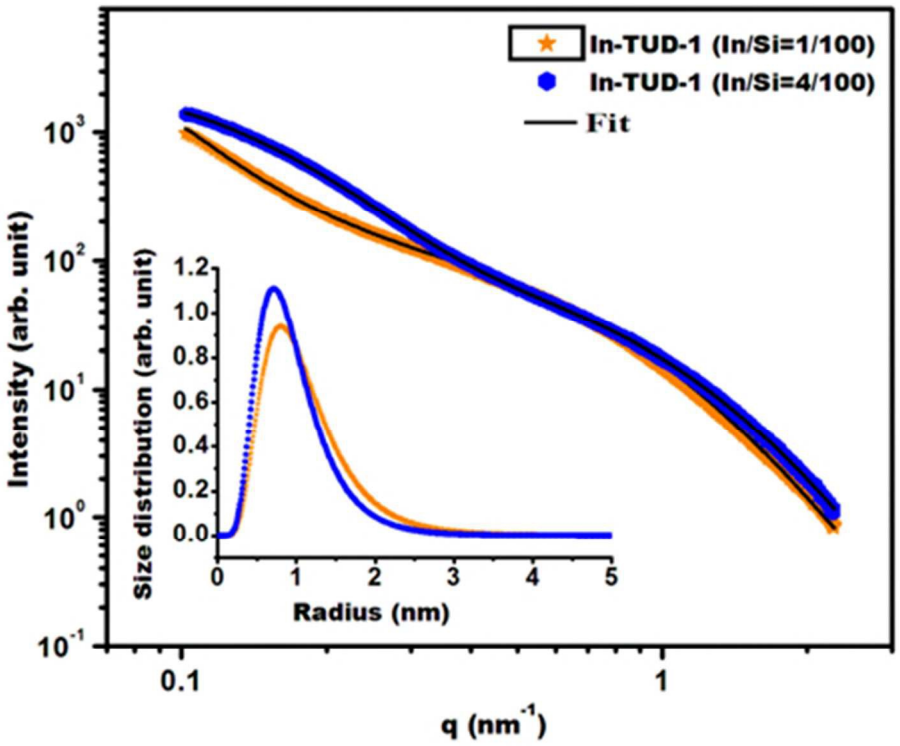

Fig. 2 Fitting of the model to the experimental SAXS data. Solid line represents the fit in each case.
39x32mm (300 x 300 DPI)

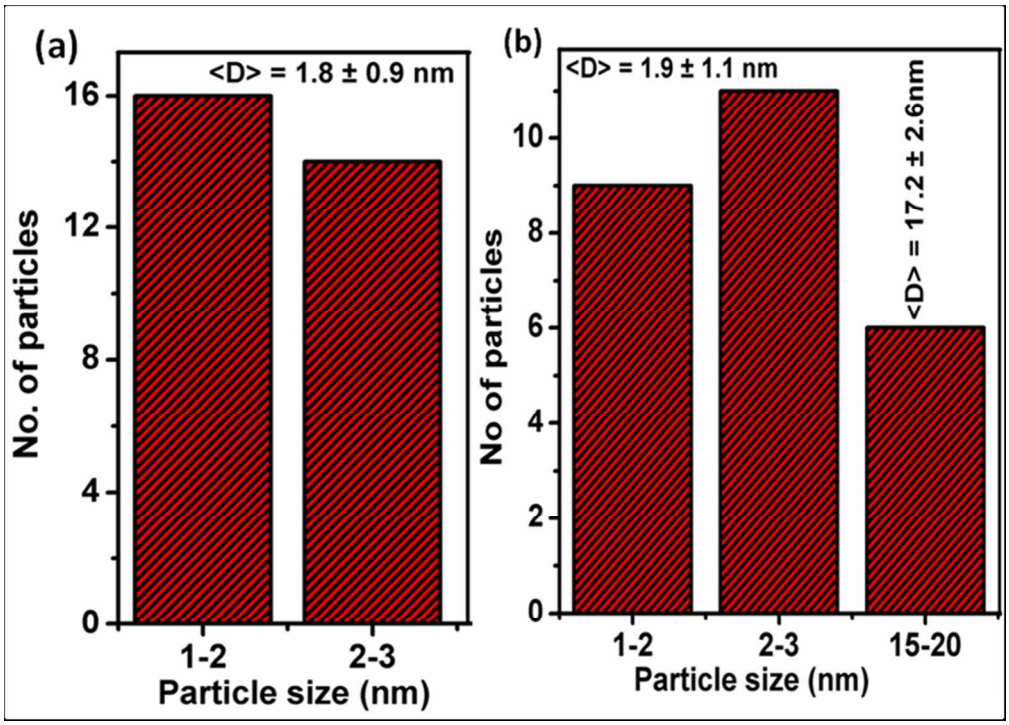

Fig. 3 Particle size distribution of In-TUD-1 (a) In/Si = 1/100 and (b) In/Si = 4/100 catalysts as obtained from HRTEM analysis
165x117mm (141 x 142 DPI)

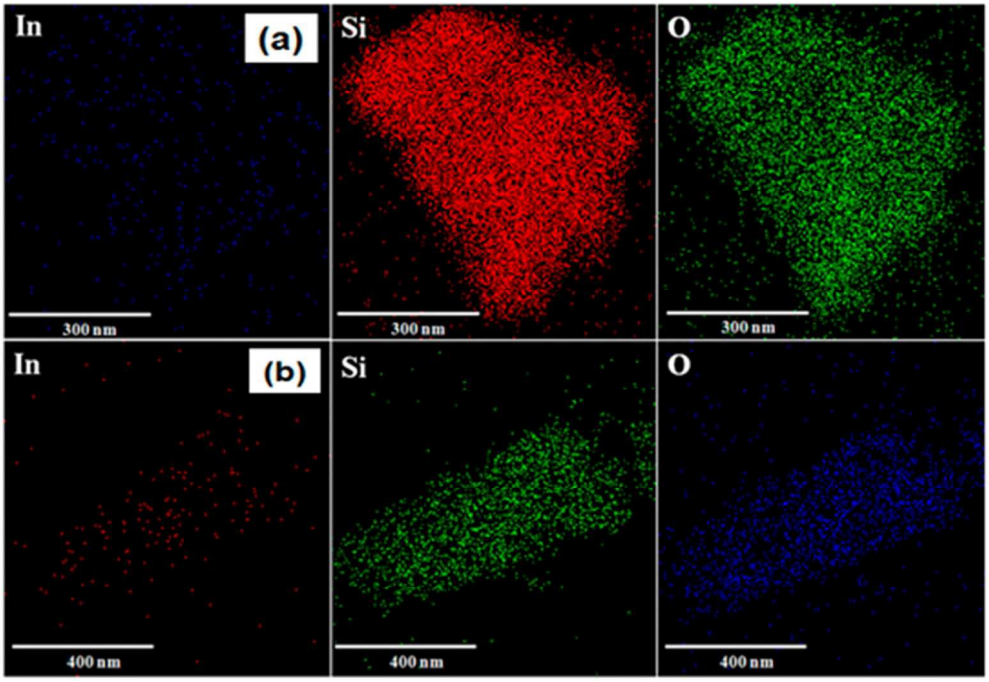

Fig. 4 Elemental mapping by STEM analysis of (a) In-TUD-1 (In/Si = 1/100), (b) In- TUD-1 (In/Si = 4/100) catalysts.
46x32mm (300 x 300 DPI)

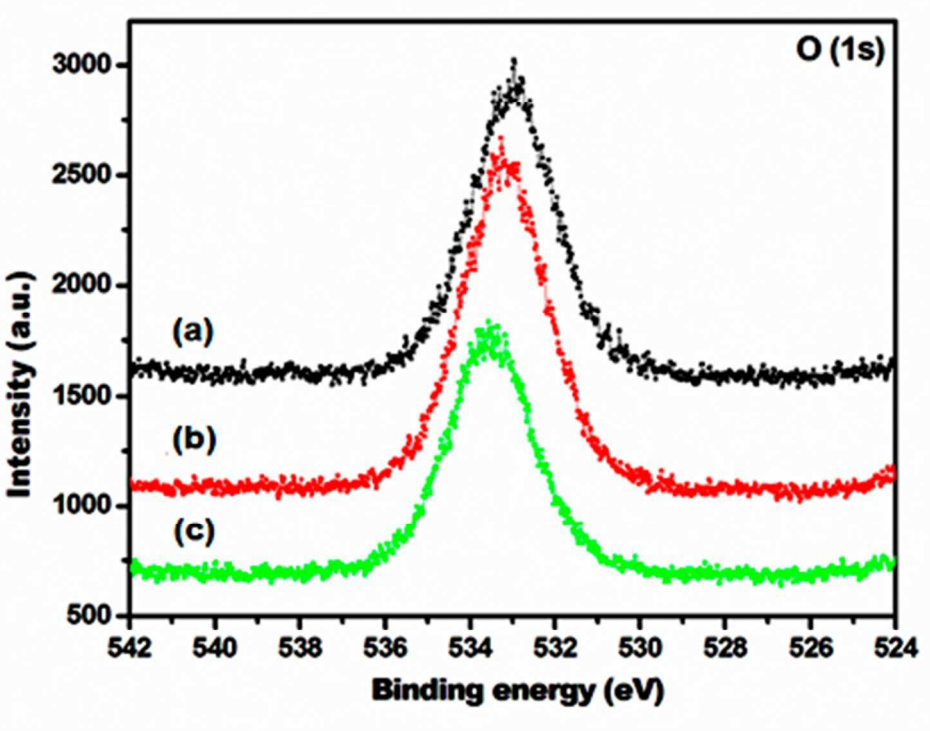

Fig. 5 The O (1s) core level XPS spectra of (a) TUD-1 (b) In-TUD-1 (In/Si = 1/100) (c) In-TUD-1 (In/Si = 4/100) catalyst.
39x31mm (300 x 300 DPI)

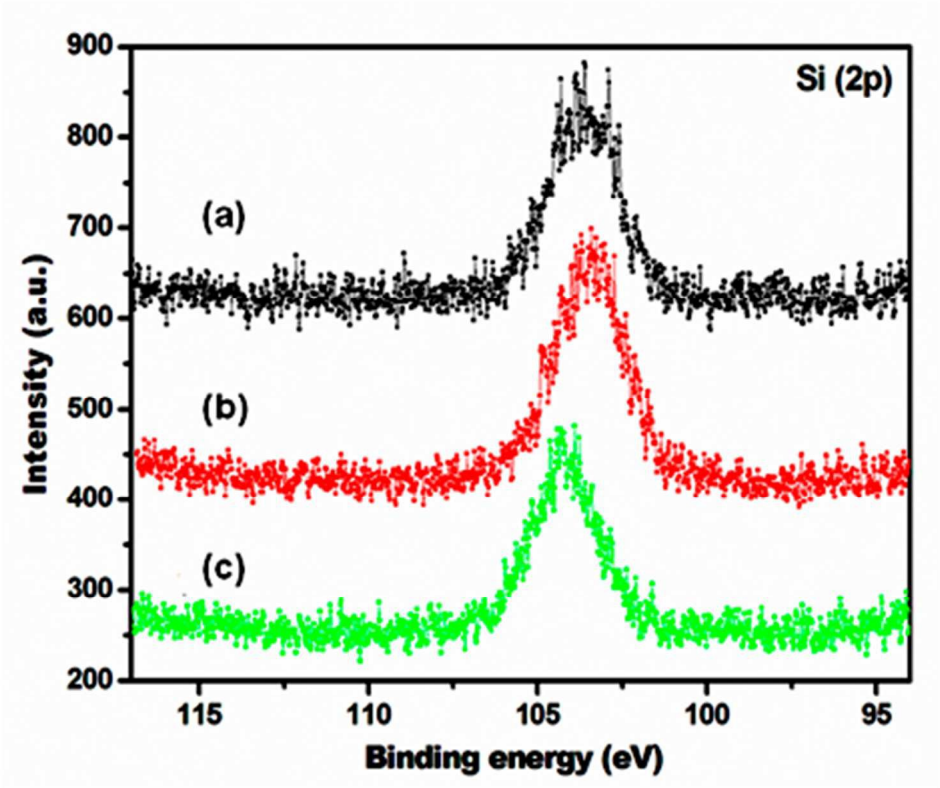

Fig. 6 Si (2p) core level XPS spectra of (a) TUD-1 (b) In-TUD-1 (In/Si = 1/100) (c) In-TUD-1 (In/Si = 4/100) catalyst.
39x33mm (300 x 300 DPI)

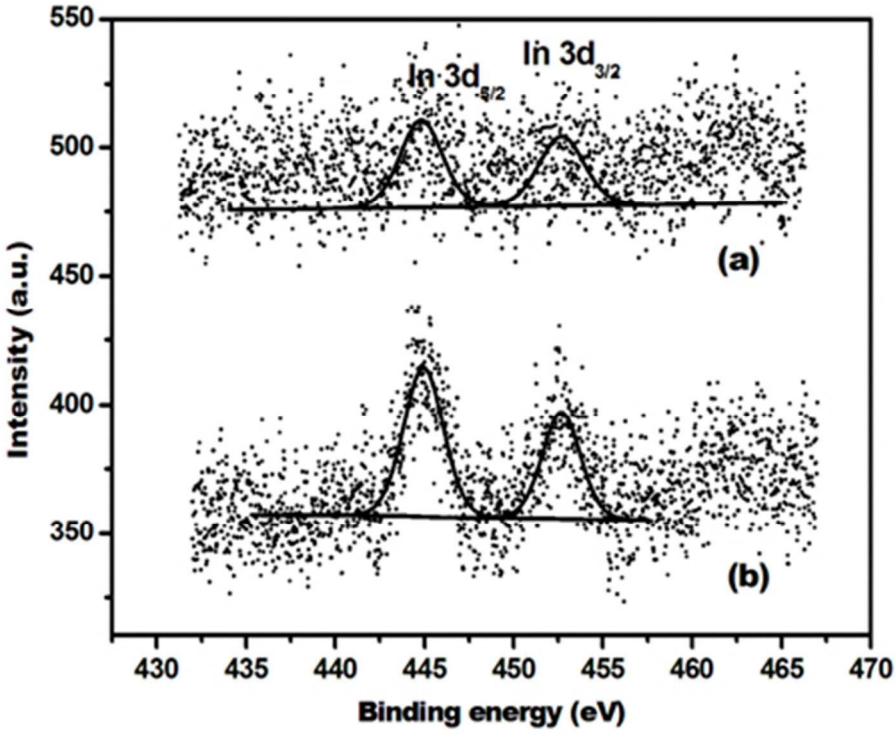

Fig. 7 In (3d) core level XPS spectra of (a) In-TUD-1 (In/Si = 1/100) (b) In-TUD-1 (In/Si = 4/100) catalysts
38x31mm (300 x 300 DPI)

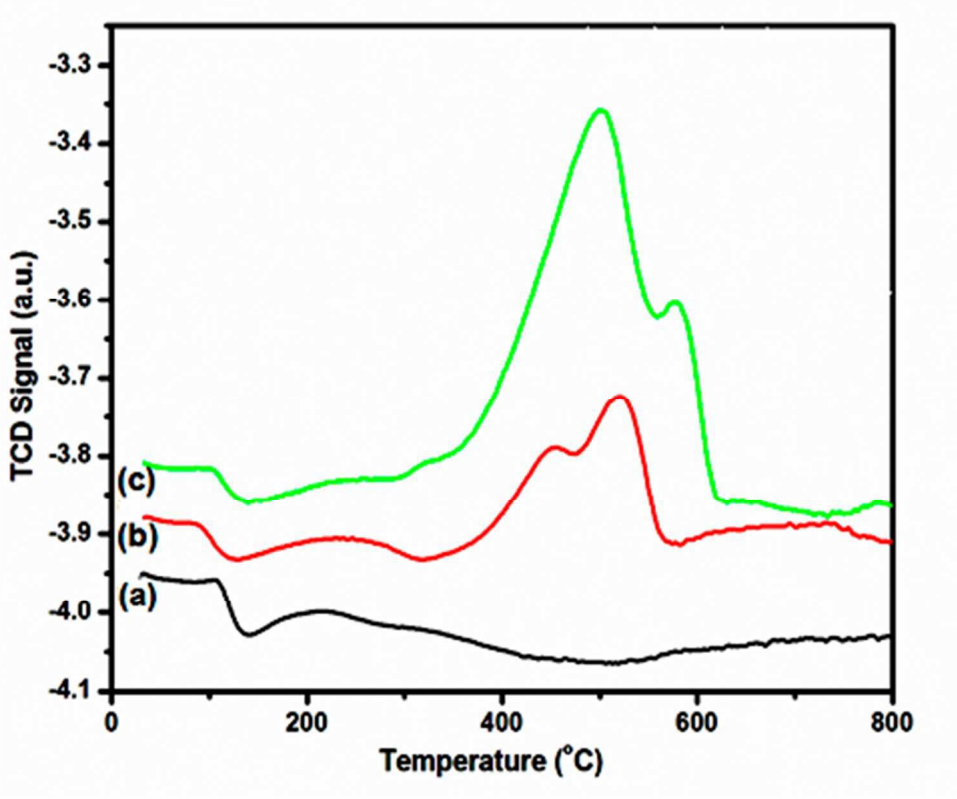

Fig. 8 The H2-TPR profiles of (a) TUD-1 (b) In-TUD-1 (In/Si = 1/100) (c) In-TUD-1 (In/Si = 4/100) catalysts.
40x34mm (300 x 300 DPI)

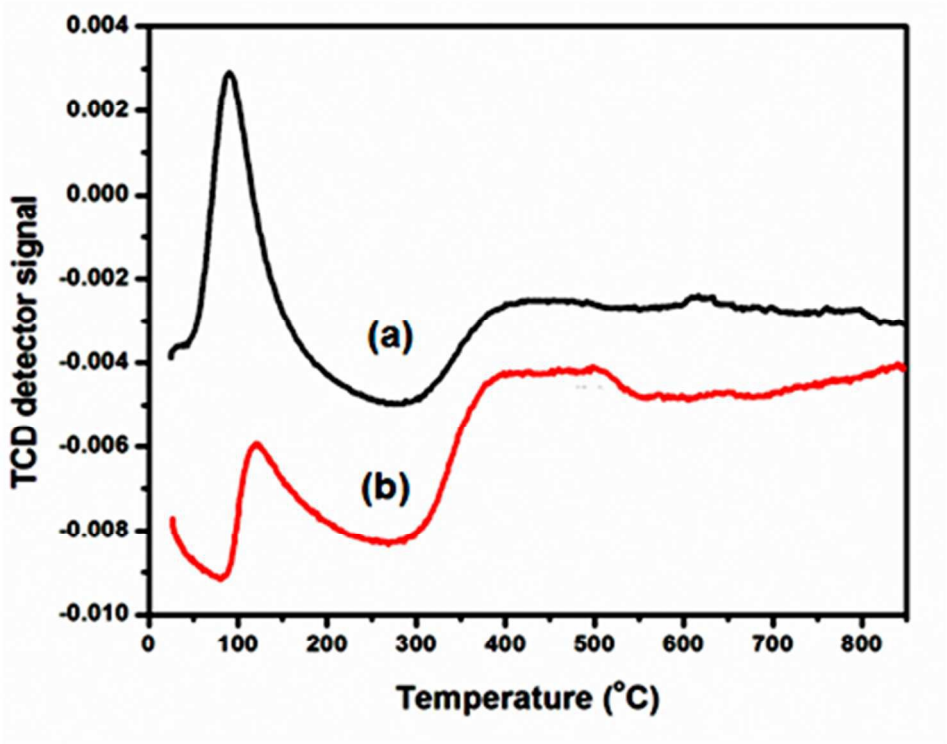

Fig. 9 The TPO profile of (a) In-TUD-1 (In/Si = 1/100), (b) In-TUD-1 (In/Si = 4/100) catalysts.
40x31mm (300 x 300 DPI)

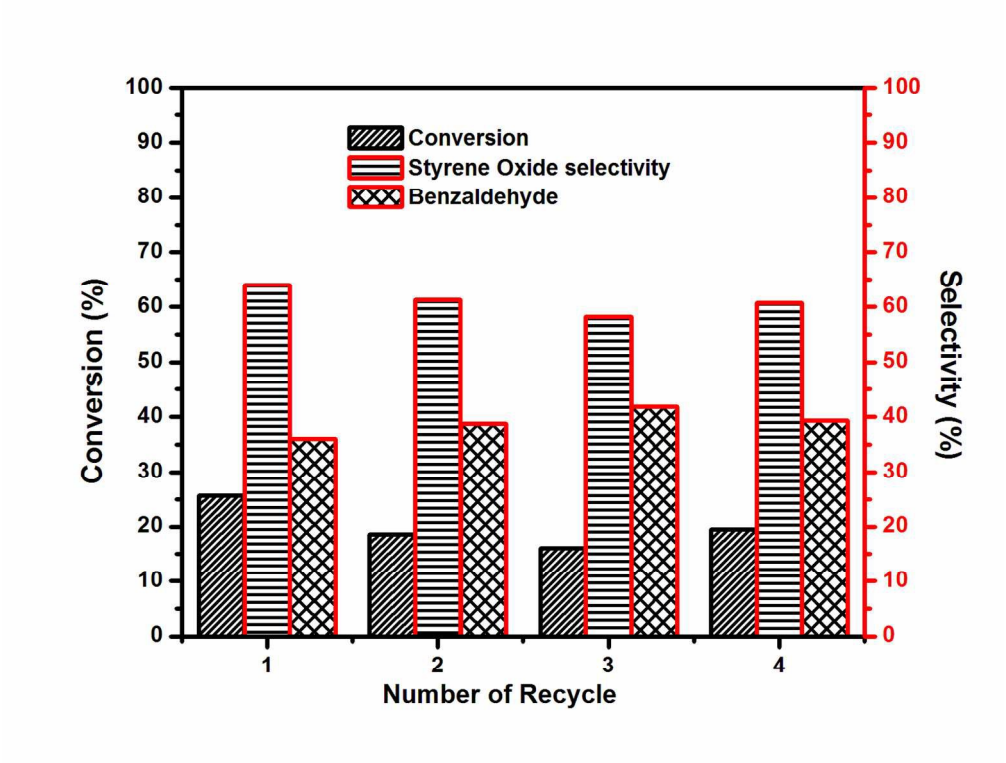

Fig. 10 Activity results of regenerated In-TUD-1 (In/Si = 1/100) catalyst for styrene epoxidation reaction.
270x206mm (150 x 150 DPI)

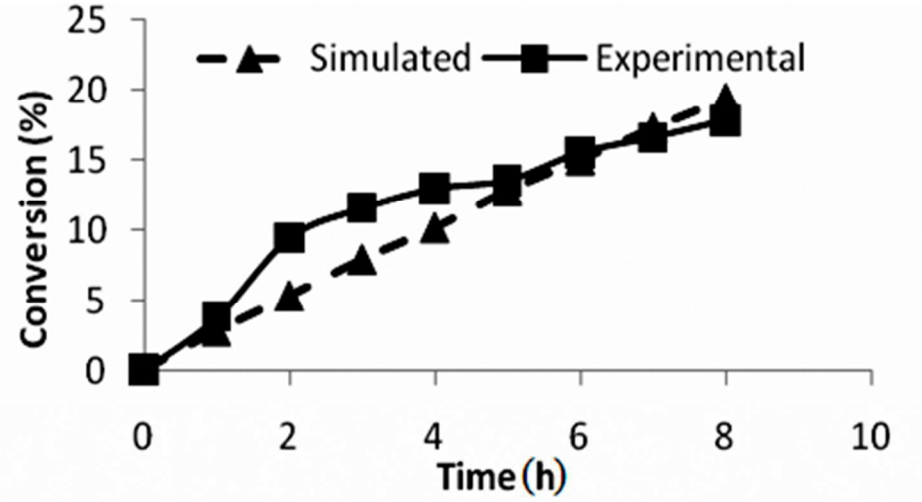

Fig. 11 Plot of Simulated and Experimental conversion (%) vs. Time (h) for styrene epoxidation reaction in a batch reactor.
39x21mm (300 x 300 DPI)

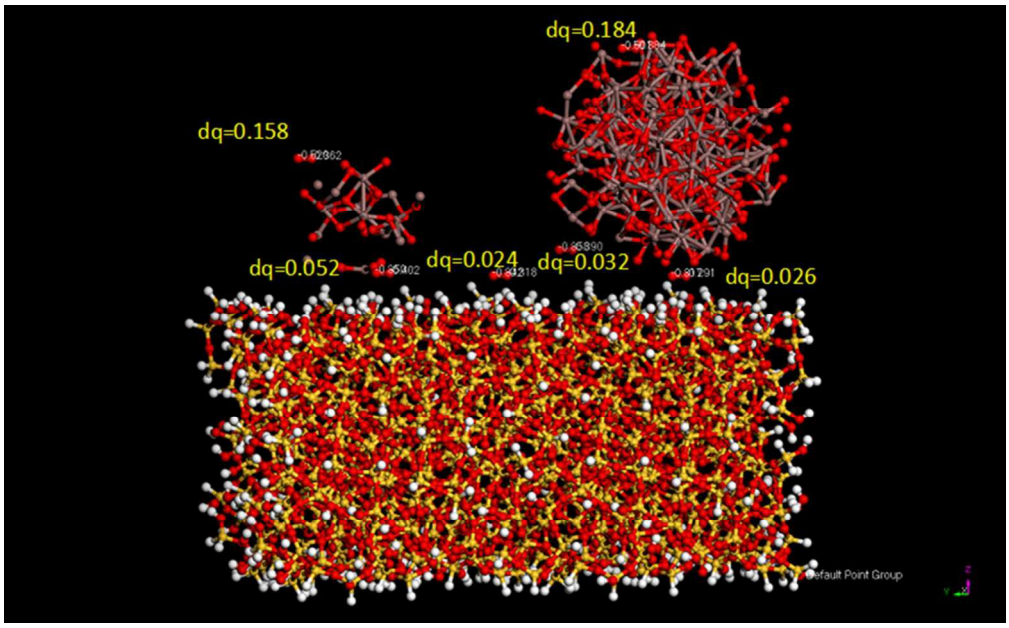

Fig. 12 The optimized structure for O2 as adsorbate on SiO2 surface with In2O3 nanoparticle along with partial charges on the atoms of adsorbed oxygen.
141x87mm (150 x 150 DPI)